In situ Controllable Growth of Prussian Blue Nanocubes on Reduced Graphene Oxide: Facile Synthesis and Their Application as Enhanced Nanoelectrocatalyst for H_2O_2 Reduction

Linyuan Cao,[†,‡] Yanlan Liu,[†,‡] Baohua Zhang,[†] and Lehui Lu*[,†]

State Key Laboratory of Electroanalytical Chemistry, Changchun Institute of Applied Chemistry, Chinese Academy of Sciences, 5625 Renmin Street, Changchun 130022, P. R. China, Graduate School of the Chinese Academy of Sciences, Beijing 100039, P. R. China

ABSTRACT As a single-atom-thick carbon material with high surface area and conductivity, graphene provides an ideal platform for designing composite nanomaterials for high-performance electrocatalytic or electrochemical devices. Herein, we demonstrated a facile strategy for controllably growing high-quality Prussian blue nanocubes on the surface of reduced graphene oxide (PBNCs/rGO), which represents a new type of graphene/transition metal complex heterostructure. The merit of this method is that the composite nanomaterials could be produced directly from GO in an in situ wet-chemical reaction, where the reduction of GO and the deposition of PBNCs occurred simultaneously. The obtained composite nanomaterials were characterized by transmission electron microscopy (TEM), X-ray photoelectron spectroscopy (XPS), X-ray diffraction (XRD), thermogravimetric analysis (TGA), Raman spectroscopy, and electrochemical techniques. It was found that uniform PBNCs with controlled size and good dispersion were directly grown on the surface of graphene nanosheets. Moreover, we also investigated the performance of PBNCs/rGO nanocomposites as amperometric sensor toward reduction of H_2O_2. Such a sensor showed a rapid and highly sensitive response to H_2O_2 with a low detection limit (45 nM), which might find promising applications in developing a new type of enzymeless biosensor.

KEYWORDS: graphene • Prussian blue • nanocube • hydrogen peroxide • electrocatalyst • biosensor

INTRODUCTION

Hybrid nanomaterials have attracted wide attention because of their unique optical, electrical, magnetic, and chemical properties that are substantially different from those of each component (1 –10). The rational design of such heterostructures can lead to novel functionalities that can be tailored to fit a specific application (1−10). A pressing example to demonstrate this is graphene-based hybrid nanomaterial, which has gained even more interest because of graphene's unique nanostructure and excellent properties, including high conductivity (1×10^3 to 1×10^4 S/m), high surface area (~2600 m^2/g), tunable band gap, high elasticity, etc. (11−14). Furthermore, the ability of graphene to promote the electron-transfer reactions has made them more attractive for use as a two-dimensional (2D) catalyst support than graphene oxide (15−17). Thus far, many graphene-based nanocomposites (such as metal/graphene, semiconductors/graphene, polymer/graphene, and metal oxides/graphene) have been designed toward applications in catalyst and optical devices, sensor, and so on (18−22). For example, Pt/graphene nanocomposite has been used as electrocatalytic material for methanol oxidation, showing better performance than Pt/carbon nanotube (Pt/CNT) composites and commercial E-TEK Pt/C catalysts (18c). Kamat et al. (19a) and Li et al. (19b) have synthesized TiO_2/chemically converted graphene (TiO_2/CCG), respectively, which displayed excellent photocatalytic activity for degradation of organic dyes.

Because its high activity toward the reduction of hydrogen peroxide, Prussian blue (PB) has been recognized as an "artificial enzyme peroxidase" for constructing electrochemical biosensors (23, 24). To realize these applications, high-quality active supports are usually required for the immobilization of PB. Thus, much endeavor has been devoted to fabricating new supports that can improve the sensor's stability and activity (25, 26). Among these investigated support materials, CNTs have been a focus of research because of the unique stability and ion-loading capacity. Nevertheless, when constructing PB/CNTs composites electrochemical sensors, multistep processes are usually required to prepare and purify CNTs or presynthesize PB nanoparticles (27), which limited their applications to a large extent. Therefore, more efforts are still needed to design novel PB-based nanocomposites and develop simple synthesis method.

* Corresponding author. Fax: (+86) 431-85262406. Tel: (+86) 431-85262418. E-mail: lehuilu@ciac.jl.cn.

Received for review April 27, 2010 and accepted July 6, 2010

† Changchun Institute of Applied Chemistry, Chinese Academy of Sciences.

‡ Graduate School of the Chinese Academy of Sciences.

DOI: 10.1021/am100372m

Scheme 1. Procedure for the Fabrication of PBNCs/rGO Nanocomposites

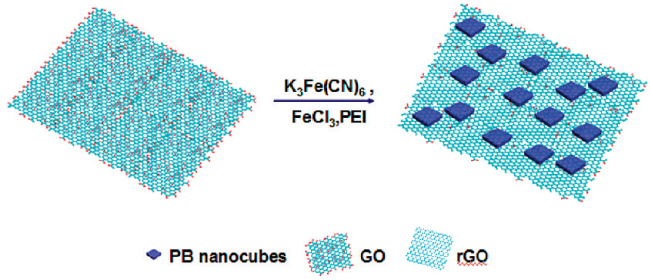

Inspired by the remarkable properties of graphene and its relative easy preparation approach, we reason that when combined with PB nanocrystals, graphene-based nanomaterials may find important functions in the applications of fabricating amperometric biosensors. However, we are not aware of publications on the utilization of reduced graphene oxide (rGO) as substrate for in situ growing PB nanocrystals with controllable size. A possible reason is the absence of facile method for controllably growing PB nanocrystals on the surface of rGO and avoiding irreversible agglomerates of the graphene sheets in the synthesis process. Herein, a facile strategy was demonstrated for in situ growth of PB nanocubes on the surface of rGO nanosheets using polyethyleneimine (PEI) as reductant (Scheme 1). The merit of this method is that the nanocomposites could be produced directly from GO in an in situ wet-chemical reaction, where the reduction of GO and the deposition of PBNCs occurred simultaneously. As a new type of transition metal complex/graphene heterostructure, it processes several important benefits. First, the in situ wet-chemical growth route provides a desirable platform for constructing hybrid nanomaterials with improved properties. Second, the loading and size of PB nanocubes on the surface of graphene could be simply controlled by changing the concentration of PB precursors, resulting in the tunable catalytic properties. Importantly, the resulting nanocomposites can be used as electrode materials for constructing electrochemical sensors, exhibiting high sensitivity and long-term stability toward the reduction of H_2O_2.

EXPERIMENTAL SECTION

Reagents. Graphite power (99%) was purchased from Shanghai Chemical Factory (Shanghai, China). Polyethyleneimine (PEI, $M_n = 423$) was obtained from Aldrich. Unless otherwise specified, hydrogen peroxide and other reagents and materials involved were obtained commercially from the Beijing Chemical Reagent Plant (Beijing, China) and used as received without further purification. All aqueous solutions were prepared with ultrapure water from a Milli-Q Plus system (Millipore).

Preparation of Graphene Oxide. Graphite oxide was synthesized using a modified Hummer's method (28), starting from graphite powders. Then, exfoliation of graphite oxide to graphene oxide (GO) was achieved by ultrasonication for 60 min. Subsequently, the as-prepared brown dispersion was subjected to 10 min of centrifugation at 3000 rpm to remove any unexfoliated graphite oxide (an extremely small amount). Finally, a homogeneous GO aqueous dispersion (0.5 mg/mL) was obtained.

Preparation of Chemically Converted Graphene. CCG was prepared using ammonia and hydrazine as reducing agents according to the literature (29). Briefly, a stable dispersion of exfoliated GO sheets (0.5 mg/mL, 50 mL) was mixed with hydrazine hydrate (50%, 35 μL) and ammonia (28%, 180 μL), and heated under reflux at 95 °C for about 1 h. After reduction, a homogeneous black dispersion with a small amount of black precipitate was obtained. Successively, this dispersion was filtered to remove the precipitate and yield a stable black aqueous dispersion of CCG (0.5 mg/mL).

Preparation of Prussian Blue Nanocubes. PBNCs were prepared according to Dong's method (30). In a typical experiment, 10 mL of 5 mM $FeCl_36 \cdot H_2O$ (pH 1.1) and 1 mL of 3% PEI were added to 10 mL of 5 mM $K_3Fe(CN)_6$ (pH 1.1) solution under stirring; the mixture was then heated and refluxed for about 3 h. The final mixture was collected by centrifugation and washed with ultrapure water three times, and then the product was redispersed in 10 mL water.

Preparation of Reduced Graphene Oxide. To prepare rGO, a stable dispersion of exfoliated GO sheets (0.5 mg/mL, 50 mL, pH 1.1) was mixed with PEI (3%, 1 mL) and heated under reflux at 135 °C for about 3 h. The obtained black dispersion was washed several times by ultrapure water, and collected by centrifugation. The final product was dried in air at room temperature.

Preparation of Prussian Blue Nanocubes/Reduced Graphene Oxide. Ten mL of 5 mM $FeCl_36 \cdot H_2O$ (pH 1.1), 1 mL of 3% PEI, and 10 mL of 5 mM $K_3Fe(CN)_6$ (pH 1.1) were added to 10 mL of GO dispersion (0.5 mg/mL, pH 1.1) under stirring, and then the mixture was heated and refluxed for 3 h. The color of the mixture gradually changed from yellow brown to dark cyan, suggesting the formation of Prussian blue nanocubes/reduced graphene oxide (PBNCs/rGO) heterostructure. The final mixture was collected by centrifugation and washed with ultrapure water three times, and redispersed in 10 mL of water for further characterization (signed sample 2). The method for preparing sample 1 and sample 3 is similar to that of sample 2, except that the volume of $K_3Fe(CN)_6$ and $FeCl_36 \cdot H_2O$ was changed to 5 and 20 mL, respectively.

Preparation of Prussian Blue Nanocubes/Chemically Converted Graphene. Ten milliliters of CCG solution (0.5 mg/mL) was mixed with 10 mL of as-prepared PBNCs solution. The final mixture was collected by centrifugation and washed with ultrapure water for three times and redispersed in 10 mL of water for further characterization (signed sample 4). In this case, the amount of PBNCs and graphene in sample 4 is consistent with that of sample 2.

Electrochemical Experiment. Prior to the surface coating, the GC electrode was polished carefully with 0.3 and 0.05 μm alumina power and rinsed with ultrapure water, followed by sonication in nitric acid (1:1), acetone, and water successively. The electrode was allowed to dry under nitrogen. For H_2O_2 redox reaction, 5 μL of PBNCs/rGO or PBNCs or CCG or the mixture of PBNCs/CCG dispersion was dropped on the surface of the GC electrode and dried in air before use.

Instruments. Powder X-ray diffraction (XRD) analysis were performed on a D8 Advance diffractometer with Cu Kα (1.5406 Å) radiation. Transmission electron microscopy (TEM) measurements were made on a JEOL 2010 transmission electron microscopy operated at an accelerating voltage of 200 kV and the samples for TEM were prepared by placing a drop of the dispersion on the carbon-coated copper grid. Thermogravimetric analysis (TGA) of samples was performed on a Pyris Diamond TG/DTA thermogravimetric analyzer (Perkin-Elmer Thermal Analysis). Samples were heated under an air atmosphere from room temperature to 750 at 5 °C min^{-1}. XPS measurement was performed on an ESCALAB-MKII spectrometer (VG Co., United Kingdom) with Al Kα X-ray radiation as the X-ray source for excitation. Raman spectra were obtained using a Renishaw Raman system model 2000 spectrometer. The 514 nm radiation from an Ar+ ion laser was used as the excitation

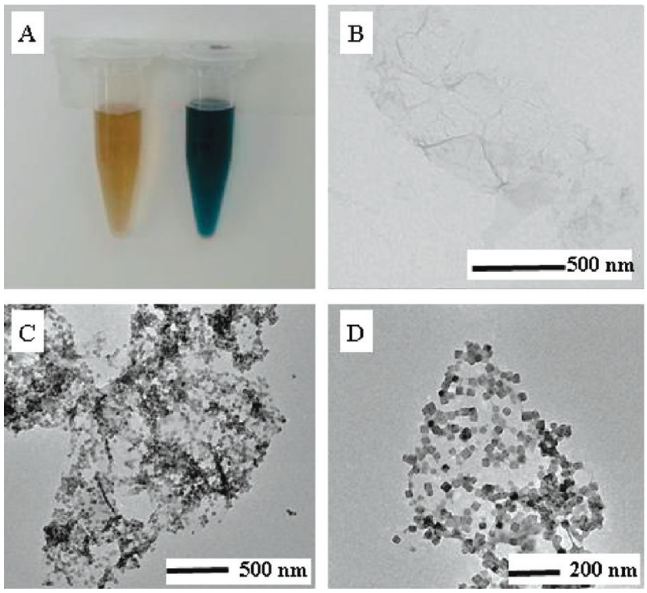

FIGURE 1. (A) Photograph of GO dispersion and PBCNs/rGO nanocomposites dispersion. TEM images of (B) GO nanosheets and (C, D) PBCNs/rGO nanocomposites.

source. Electrochemical experiments were performed with a CHI 830B electrochemical analyzer (CH Instruments, Chenhua Co., Shanghai, China). A conventional three-electrode cell was used, including a Ag/AgCl (saturated KCl) electrode as reference electrode, a platinum wire as counter electrode, and modified GC as working electrode.

RESULTS AND DISCUSSION

The proposed strategy for the fabrication of PBNCs/rGO composite was shown in Scheme 1. In the first step, the GO nanosheets were prepared by oxidizing graphite according to a modified Hummer's method (28), and subsequently redispersed in ultrapure water by ultrasonic treatment to obtain a homogeneous brown dispersion (Figure 1A). As observed in Figure 1B, the Cu gridding substrates were covered with a number of thin films ranging from 500 nm to greater than 2 μm in size, indicating that GO nanosheets have been exfoliated. Upon exfoliation the GO carried sufficient functional groups (e.g., epoxides, hydroxyl, carboxylic acids), which might provide active sites for anchoring external nanoparticles (31). In the second step, the GO nanosheets were used as template to grow PB nanocubes for producing PBNCs/rGO nanocomposite via an in situ reduction process. An obvious color change of the dispersion from brown to dark cyan revealed that PBNCs/rGO was successfully obtained (Figure 1A). The morphology of the as-prepared PBNCs/rGO composites was investigated by transmission electron microscopy (TEM). It is observed that well-separated nanocrystals with a size ranging from 38 to 42 nm spread out on or below the surface of rGO nanosheets (Figure 1C,D), which guaranteed efficient electrochemical properties of PBNCs/rGO nanocomposites. The corresponding selected area electron diffraction (SAED) of the PB nanocrystals (see Figure S1 in the Supporting Information) demonstrated that the cubic PB nanostructures were single-crystalline and enclosed by {200} and {220} facets.

To ascertain the structure and composition of the nanocomposite, a series of analysis were performed. XRD patterns of the samples prepared with different weight ratio of PB precursors and rGO were displayed in Figure 2. All reflections can be indexed as a pure face-centered-cubic phase of Prussian blue with space group *Fm*3*m* (No. 225) (JCPDS card 73−0687). The peaks located at $2\theta = 17.69$, 25.00, 35.56, 39.89, 51.12, 54.36, and 57.63° were assigned to the (200), (220), (400), (420), (440), (600), and (620) reflections of the PB, respectively (32). It was worth noting that with gradually increasing the weight ratio of PB precursors and rGO, the mean diameters of the nanocubes were determined from the width of the strongest diffraction lines ((200) diffraction line) by using the Debye−Scherrer formula to be about 32.2, 35.3, and 44.2 nm, respectively. In addition, no obvious diffraction peak attributed to graphite was found, which indicated that the stacking of rGO sheets remained disordered (33).

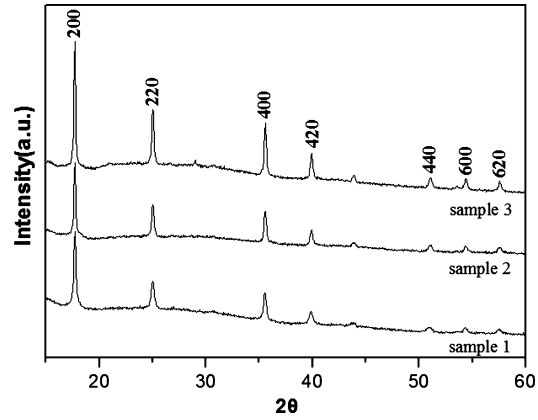

FIGURE 2. XRD patterns of PBNCs/rGO nanocomposites at different initial $K_3Fe(CN)_6$:GO sheets weight ratio. sample 1, 15; sample 2, 33; sample 3, 60.

XPS analysis provides detailed information on the chemical composition of the as-prepared nanocomposite. The fully scanned spectra demonstrated that C, and O elements existed in GO sample (Figure 3A), whereas after refluxing in the presence of $FeCl_3$, $K_3Fe(CN)_6$, and PEI, the XPS spectrum indicated the presence of N, and Fe elements in the composites, besides C and O (Figure 3B). To further understand the electronic states of the elements, we paid more attention to the higher-resolution spectra. The binding energies of $Fe2p_{3/2}$ and $Fe2p_{1/2}$ were observed at 711.3 and 724.8 eV, respectively, which originated from the presence of Fe^{3+} (Figure 3C) (34). The peak at 708.3 eV can be assigned to Fe $2p_{3/2}$ of $[Fe(CN)_6]^{4-}$. In the case of N1s, the main peak of the N1s core-level spectra was fitted with three components at 401.7, 399.5, and 397.4 eV, signifying the existence of PEI and C−N ($[Fe(CN)_6]^{4-}$) in the composites (Figure 3D) (35). On the basis of the higher-resolution spectra of N1s and Fe 2p, we could conclude that PB nanocrystals were successfully synthesized. Notice that the C 1s spectrum for GO displayed strong $C_{epoxide}$ signal, which decreased in intensity upon loading with PB. This revealed the proportion of oxygen-containing functional groups on GO was reduced during the refluxing process in the presence of PEI (36). The direct evidence for the reduction of GO could be obtained from Figure S2. Besides, the C1s spectrum of PBNCs/rGO also displayed the presence of C−C (284.8 eV), C═O (287.6

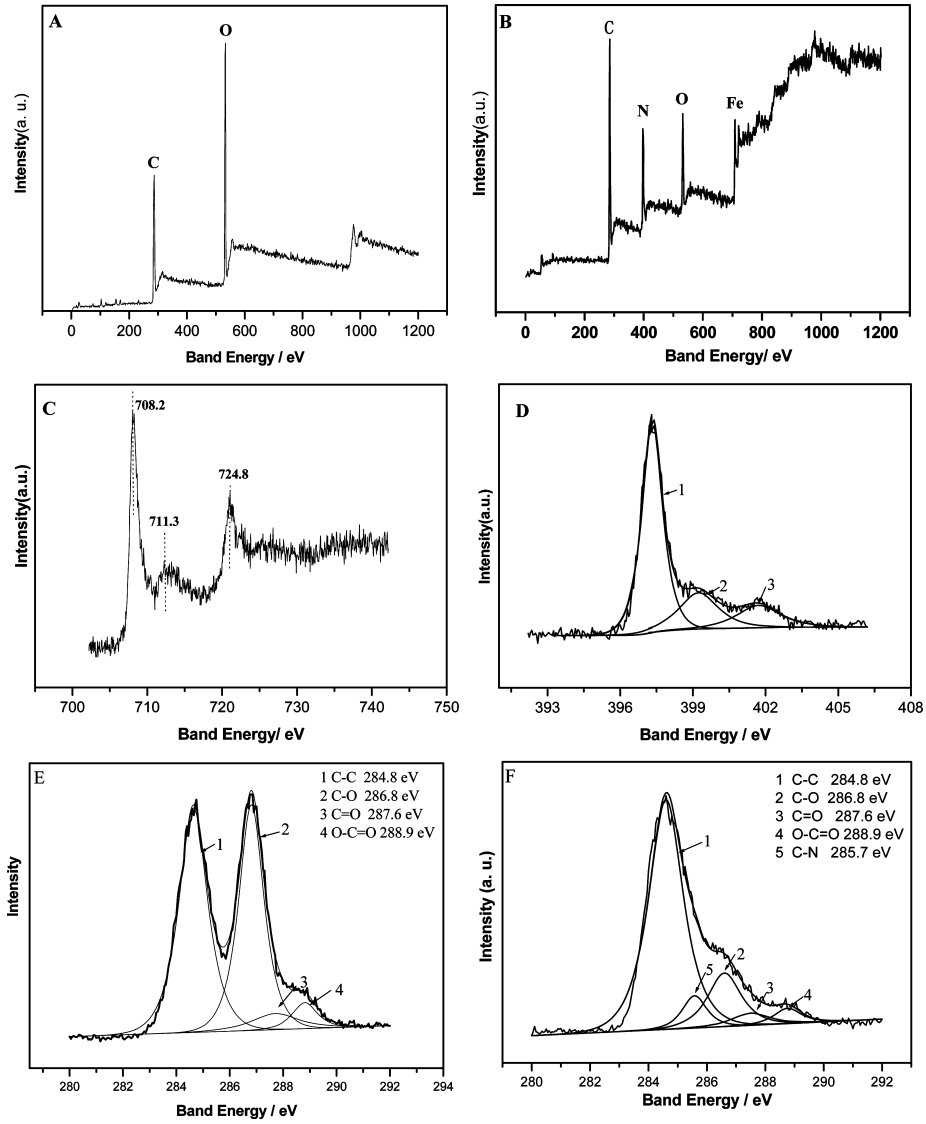

FIGURE 3. XPS spectra of GO and PBNCs/rGO (sample 2). (A) GO; (B) PBNCs/rGO; (C) Fe 2p spectrum of PBNCs/rGO; (D) N 1s spectrum of PBNCs/rGO; (E) C 1s of GO; (F) C1s of PBNCs/rGO.

eV), and O−C═O (288.9 eV) species (Figure 3E,F). The polar groups (C═O, O−C═O) might provide strong interaction with the cleaned GC electrode surface, leading to the formation of stable modified electrode (37).

Further support for the formation of PBNCs/rGO composite can be provided by TGA analysis (see Figure S3 in the Supporting Information). Both GO and nanocomposite samples suffered from a slight loss mass on heating even below 100 °C, most likely because of the loss of water. With the increase in temperature, a significant mass drop around 170 °C was observed in the TGA curve for GO, which could be assigned to the decomposition of the labile oxygen-containing functional groups (38), and this feature accounted for 36.9% of the initial mass, giving a $C_{graphene}$/O ratio of 1.63, well consistent with that analysis of XPS. The TGA curve for PBNCs/rGO featured the similar mass loss; however, the curve showed a gradual mass loss spanning the 250−500 °C range, which was attributed to the loss of uncoordinated and coordinated water present in PBNCs (39) and yielded a weight loss of 17.7%. When the temperature increased to 550 °C, the drops in the two curves were ascribed to pyrolysis of the carbon skeleton (40). The above results supported the conclusion that the PBNCs/rGO nanocomposites were successfully fabricated through the in situ reduction wet-chemical method.

Considering the strong bonding between rGO and PBNCs, Raman spectroscopy was employed to check the special interaction in the composites (see Figure S4 in the Supporting Information). In all spectra, two prominent peaks were clearly visible, corresponding to the so-called D and G bands at about 1359 and 1600 cm^{-1}, respectively. The D band arose from vibrations of carbon atoms with dangling bonds in plane terminations of disordered graphite; while the G band was associated with the vibration of sp^2-bonded carbon atoms (41). The intensity ratio of D and G band (I_D/I_G ratio) was proportional to the number of defect sites in graphite carbon. For our samples, the I_D/I_G ratio of PBNCs/rGO nanocomposite and GO was 1.03 and 0.82, respectively, reflecting the decrease in the average size of the in-plane sp2 domains and a partially ordered crystal structure of rGO

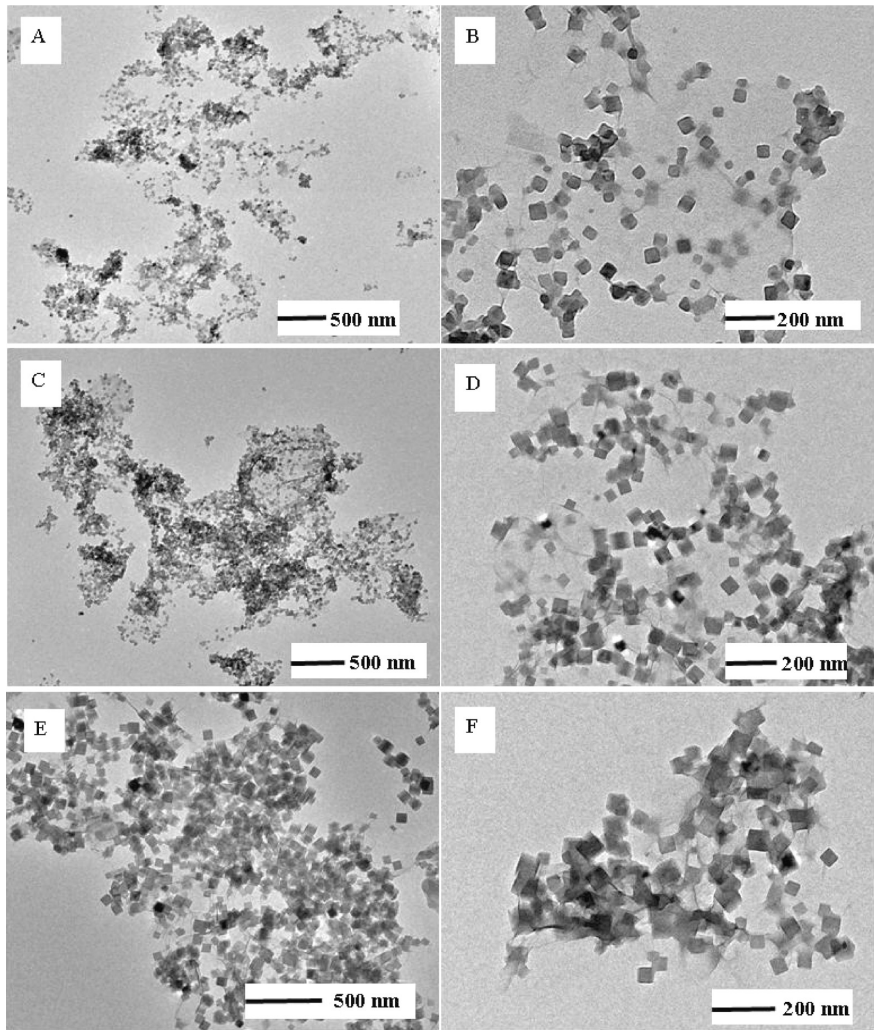

FIGURE 4. TEM images of PBCNs/rGO nanocomposites with different initial $K_3Fe(CN)_6$:GO sheets weight ratio. (A, B) sample 1; (C, D) sample 2; (E, F) sample 3.

(17, 42), and can be explained if new graphitic domains were created that are smaller in size than the ones present in GO before reduction, but more numerous in number (42). Furthermore, the I_D/I_G ratio of rGO was also calculated as 1.17, close to that of PBNCs/rGO, which agreed well with the Raman spectra of the GO reduced by hydrazine, AA, and phenyhydrazine (43). The result further revealed that GO has been reduced by PEI during the refluxing process. Noticeable, the G band of PBNCs/rGO appeared at 1606 cm^{-1}, which was 8 cm^{-1} higher than that of pure CCG (1598 cm^{-1}). The shift of G band could be concurred with previous reports of the electrochemical doping on rGO, and with the chemical doping on CNT (44). Here, the additional PBNCs might change the carrier concentration in the plane of rGO and led to the shift of G band (45). The Raman shift of the G band for PBNCs/rGO was indicative of a chemical interaction between PBNCs and the rGO nanosheets (44).

Before more applications could be considered, additional laboratory experiments were needed to elucidate some influencing factors.

3.1. pH Value. It is well-known that Fe^{3+} is easily affected by pH, and thus pH value optimization is one of the key factors for controlling the size of PB nanocrystals on the surface of rGO. We fixed the weight ratio of $K_3Fe(CN)_6$/GO at 33, and set pH value at 1.1, 2.0, or 3.0, respectively. TEM images of the as-obtained PBNCs/rGO nanocomposites were shown in Figure S5 in the Supporting Information. On the whole, the morphology of rGO did not change much with the pH variation. However, the average size of PBNCs was affected obviously. At pH 1.1, PBNCs with size of about 40 nm were clearly visible on the surface of rGO sheets. At pH 2, the average size of PBNCs gradually grew up to 60 nm and the particle size distribution became broader than that at pH 1.1, probably due to the slight hydrolysis of Fe^{3+}. Nevertheless, further increasing the pH value to 3 led to the formation of irregular-shaped nanoparticles, revealing that the formation of cubic PB nanocrystals is dependent strongly on the pH value of the mixture. To fabricate high-quality PBNCs/rGO nanocomposites, pH 1.1 was selected for growing PB nanocrystals on the rGO nanosheets in this case.

3.2. Weight Ratio of $K_3Fe(CN)_6$/GO. The amount of PB precursor was another important factor in determining the morphologies of PBNCs. TEM images of the PBNCs/rGO nanocomposites prepared with different weight ratio of PB precursor and GO were presented in Figure 4. We found that the size and density of the PBNCs on the surface of rGO

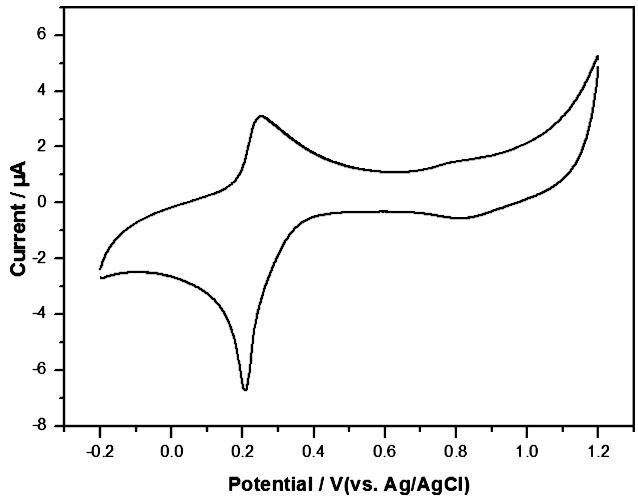

FIGURE 5. Cyclic voltammogram of a GC electrode modified with PBNCs/rGO nanocomposite (sample 2) in a 0.1 M KCl solution at 50 mV s^{-1}.

nanosheets increased simultaneously with increasing concentration of the PB precursor. When the ratio was set at 15, PBNCs with an average size of 32 nm were tightly bound to the surface of rGO, but the coverage degree was low. At the weight ratio of 33, the coverage degree of PBNCs increased obviously as compared to that produced at a lower concentration of precursors. When further increased the weight ratio to 60, the PBNCs loading was improved or even resulted in the saturation and the average size of PBNCs increased to about 50 nm. Such dependence of PBNCs coverage density on the weight ratio may provide a desirable way for controlling the microstructure of nanocomposites.

To probe other factors responsible for the synthesis of PBNCs/rGO hybrid materials in the present approach, we also conducted other control experiments. First, we replaced GO by CCG under the same experimental conditions. However, only aggregated CCG sheets rather than PBNCs/rGO composites were obtained. This result indicated that the exogenous functional groups on GO played an important role in constructing uniform hybrid composites. Also, we attempted to prepare PBNCs/rGO by mixing separately prepared PBNCs and rGO sheets instead of in situ wet-chemical reduction of GO and PB precursor, and but it failed. It was found that the former route resulted in aggregation of the PBNCs with poor dispersion on the sheets. On the other hand, the latter route resulted in well-dispersed nanocubes on the rGO sheets, suggesting that specific interaction between the PBNCs and the rGO nanosheets may be responsible for dispersion of the nanocubes (Figure S6).

With the aim of gaining further insight into the characteristic of PBNCs/rGO nanocomposites, cyclic voltammetry was performed to investigate the electrochemical behaviors of the PBNCs/rGO under 0.1 M KCl. As shown in Figure 5, the PBNCs/rGO modified GC electrode displayed the typical redox characteristics of PB. The redox pair located at ca. 0.20 V corresponded to the reduction of PB to Prussian white (PW), while the redox pair at ca. 0.9 V corresponded to the reversible conversion of PB to Berlin green (24). The potential separation of the pair of peaks (ca. 0.2 V) was only 41 mV, which was very close to the theoretical value, suggesting the fast charge transfer on the modified electrode. The effect of potential scan rate on the current peaks at ca. 0.2 V was investigated in the range 10−800 mV s^{-1}. As expected, a linear relationship between the cathodic peak current and the square root of the scan rate was observed (see Figure S7 in the Supporting Information), demonstrating the observed electrochemical reaction was a diffusion-process, in good agreement with previous reports (26, 44). The above results indicated the PBNCs/rGO nanocomposite maintained the good electrochemical activity of PB (26), which would offer an ideal platform for applications in the field of electrochemistry.

Hydrogen peroxide (H_2O_2) is an important intermediate species in many biological and environmental processes, and numerous kinds of O_2-dependent oxidases generate H_2O_2 upon the catalytic oxidation of the respective substrates (24, 46). Therefore, the accurate determination of H_2O_2 is of practical importance. By virtue of the fact that PB is usually considered as an artificial enzyme peroxides, it will be interesting to investigate whether the present PBNCs/rGO nanocomposite can be used for constructing H_2O_2 sensor with high performance. With this in mind, the performance of PBNCs/rGO nanocomposite as electrocatalysts toward the reduction of hydrogen peroxide was evaluated by cyclic voltammograms in 0.1 M PBS solution (pH 7.0) (see Figure S8 in the Supporting Information). It was found that the cathodic current increased from 1.02 to 6.42 μA with the increase of weight ratio of PB precursor/GO from 15 to 33, suggesting the electrocatalytic activity of composites could be finely tuned by controlling its weight ratio. However, when the weight ratio was higher than 33, the cathodic current was obviously decreased, which might be attributed to the weak conductivity of PB. To discern the distribution of individual components, the control experiments on GC, CCG/GC, PBNCs/GC, and PBNCs/rGO modified GC electrodes were carried out (see Figure S9A−D in the Supporting Information). The results demonstrated that the reduction of H_2O_2 on PBNCs/rGO/GC electrode has the lowest overpotential, that is, the as-prepared PBNCs/rGO/GC nanocomposite was the best electrocatalyst toward the reduction of H_2O_2 (26). Furthermore, previous studies have demonstrated that the synergistic effect between PB and CNT plays an important role in enhancing the amperometric response of H_2O_2 (26, 47). To ascertain the possible interaction between PB and rGO in the as-prepared composite, we also compared the catalytic performance of sample 2 and sample 4 at the same condition (see Figure S9E in the Supporting Information). Surprisingly, at about 0.2 V, a higher cathodic current (6.42 μA) was observed at the electrode modified by sample 2 than that of sample 4 (3.90 μA) (Figure S9F in the Supporting Information), indicating the higher electrocatalytic activity of PBNCs/rGO nanocomposite. The reason can be ascribed to the improved electronic and ionic transport capacity (44) resulting from the special interaction between rGO and PBNCs in sample 2.

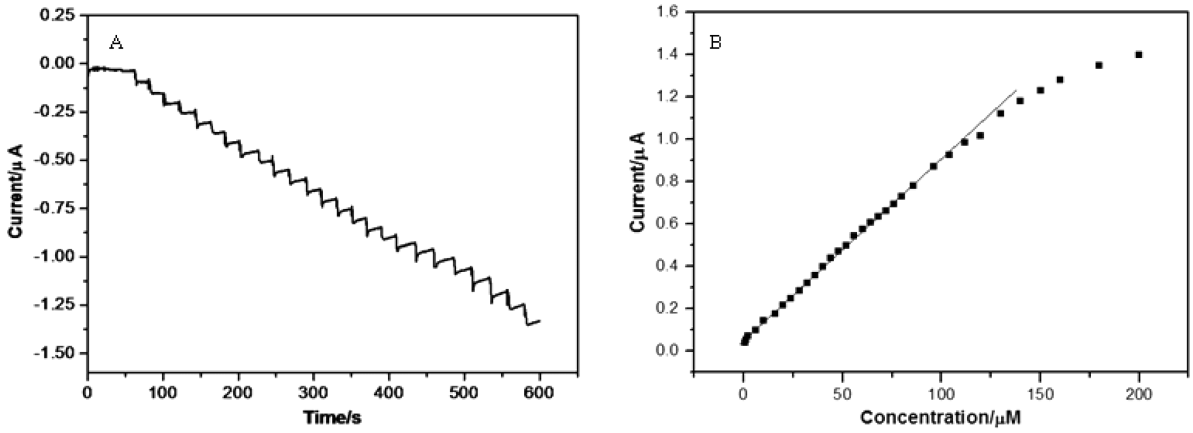

FIGURE 6. (A) Amperometric response curve of a PBNCs/rGO (sample 2) modified GC electrode at a detection potential of 0.2 V vs Ag/AgCl in a stirred PBS solution (0.1 M, pH 7.0) upon continuous injection of different concentration H_2O_2 for each step. (B) Amperometric response to H_2O_2 concentration.

Considering the excellent electrocatalytic activity of PBNCs/rGO composites toward the reduction of H_2O_2, we then proceeded to investigate the amperometric response of sample 2 to successive additions of H_2O_2 at 0.2 V (Figure 6A). With the addition of H_2O_2, a stable amperometric response could be seen on the modified electrode, presenting a very short transient response time of 5 s. A good linear correlation was found over the concentration range from 0.05−120 μM ($R^2 = 0.99$) (Figure 6B), which was wider than that at CNT/AuNPs/PB electrode (4−19.6 μM) (48). The limit of detection was 45 nM at a signal-to-noise ratio of 3, which was lower than those at PB/MCNT hybrid-based sensors (49) (0.57 μM), CNT/AuNPs/PB (3.36 μM) (48), PB/OMC composite-based sensor (1 μM), (25d), etc. The relative standard deviation (RSD) of the sensor response to 0.4 mM H_2O_2 was 3.8% for 12 successive measurements. Furthermore, the stability of the sensor was investigated by measuring voltammetric currents of the electrode. While the electrode was continuously scanned at the same conditions for 100 cycles, the as-prepared PBNCs/rGO composite could maintain its high electrocatalytic ability (that is, the peak currents decreased only4.2%). When the electrode was stored at room temperature for two weeks, the current responses toward 0.4 mM H_2O_2 maintain 90.6% of its initial response. Based on the above results, we can conclude that the prepared PBNCs/rGO hybrid nanoelectrocatalyst has a good stability for H_2O_2 detection.

CONCLUSIONS

In summary, we have developed a facile in situ wet-chemical procedure to synthesize Prussian blue nanocubes/reduced graphene oxide composites. This method provided a new route to prepare graphene-based nanocomposites. The tunable electrochemical characteristic of composites can be achieved via effectively controlling the loading and size of PBNCs on the surface of rGO sheets. Importantly, the as-prepared PBNCs/rGO could be employed as an H_2O_2 electrochemical sensor, showing a low limit detection and high sensitivity. In view of the distinguished properties of PB and rGO, these nanocomposites may find promising applications in other fields including electrochromic displays, biofuel cells, bioelectronics devices, and so on.

Acknowledgment. Financial support by the National Basic Research Program of China (973 Program 2010CB933600), the "Hundred Talents Project" of the Chinese Academy of Sciences, NSFC (20873138), and State Key Laboratory of Electroanalytical Chemistry is gratefully acknowledged.

Supporting Information Available: SAED pattern of PBNCs; XPS C1s of graphene reduced by PEI; TGA curves and Raman spectra of PBNCs/rGO composites; TEM images of PBNCs/rGO composite obtained under various synthetic conditions; plot of the peak current at ca. 0.2 V versus the scan rate; CVs of PBNCs/rGO modified GC, GC, CCG/GC, and PBNCs/GC electrodes toward 0.4 mM H_2O_2 (PDF). This material is available free of charge via the Internet at http://pubs.acs.org.

REFERENCES AND NOTES

(1) Cozzoli, P. D.; Pellegrino, T.; Manna, L. *Chem. Soc. Rev.* **2006**, *35*, 1195–1208.
(2) Kickelbick, G. *Hybrid Materials: Synthesis, Characterization and Application*; Wiley-VCH: Weinheim, Germany, 2007.
(3) Sanchez, C.; Soler-Illia, G. J. D. A.; Ribot, F.; Lalot, T.; Mayer, C. R.; Cabuil, V. *Chem. Mater.* **2001**, *13*, 3061–3083.
(4) Stankovich, S.; Dikin, D. A.; Dommett, G. H. B.; Kohlhaas, K. M.; Zimney, E. J.; Stach, E. A.; Piner, R. D.; Nguyen, S. T.; Ruoff, R. S. *Nature* **2006**, *442*, 282–286.
(5) Compton, O. C.; Nguyen, S. T. *Small* **2010**, *6*, 711–723.
(6) Plante, I. J.; Habas, S. E.; Yuhas, B. D.; Gargas, D. J.; Mokari, T. *Chem. Mater.* **2009**, *21*, 3662–3667.
(7) Zhang, B. H.; Wang, H. S.; Lu, L. H.; Ai, K. L.; Zhang, G.; Cheng, X. L. *Adv. Funct. Mater.* **2008**, *18*, 2348–2355. Jia, J. B.; Cao, L. Y.; Wang, Z. H. *Langmuir* **2008**, *24*, 5932–5936.
(8) Lu, L. H.; Eychmuller, A. *Acc. Chem. Res.* **2008**, *41*, 244–253.
(9) Lu, L. H.; Capek, R.; Kornowski, A.; Gaponik, N.; Eychmuller, A. *Angew. Chem., Int. Ed.* **2005**, *44*, 5997–6001.
(10) Zhao, X. M.; Zhang, B. H.; Ai, K. L.; Zhang, G.; Cao, L. Y.; Liu, X. J.; Sun, H. M.; Wang, H. S.; Lu, L. H. *J. Mater. Chem.* **2009**, *19*, 5547–5553.
(11) Geim, A. K.; Novoselov, K. S. *Nat. Mater.* **2007**, *6*, 183–191.
(12) Bunch, J. S.; Van Der Zande, A. M.; Verbridge, S. S.; Frank, I. W.; Tanenbaum, D. M.; Parpia, J. M.; Craighead, H. G.; McEuen, P. L. *Science* **2007**, *315*, 490–493.
(13) Park, S.; Ruoff, R. S. *Nat. Nanotechnol.* **2009**, *4*, 217–224.
(14) Rao, C. N. R.; Sood, A. K.; Subrahmanyam, K. S.; Govindaraj, A. *Angew. Chem., Int. Ed.* **2009**, *48*, 7752–7778.

(15) Shang, N. G.; Papakonstantinou, P.; McMullan, M.; Chu, M.; Stamboulis, A.; Potenza, A.; Dhesi, S. S.; Marchetto, H. *Adv. Funct. Mater.* **2008**, *18*, 3506–3514.

(16) Tang, L. H.; Wang, Y.; Li, Y. M.; Feng, H. B.; Lu, J.; Li, J. H. *Adv. Funct. Mater.* **2009**, *19*, 2782–2790.

(17) Zhou, M.; Zhai, Y. M.; Dong, S. *J. Anal. Chem.* **2009**, *81*, 5603–5613.

(18) (a) Scheuermann, G. M.; Rumi, L.; Steurer, P.; Bannwarth, W.; Mulhaupt, R. *J. Am. Chem. Soc.* **2009**, *131*, 8262–8270. (b) Yoo, E.; Okata, T.; Akita, T.; Kohyama, M.; Nakamura, J.; Honma, I. *Nano Lett.* **2009**, *9*, 2255–2259. (c) Guo, S. J.; Dong, S. J.; Wang, E. K. *ACS Nano* **2010**, *4*, 547–555.

(19) (a) Williams, G.; Seger, B.; Kamat, P. V. *ACS Nano* **2008**, *2*, 1487–1491. (b) Zhang, H.; Lv, Y. M.; Wang, Y.; Li, J. H. *ACS Nano* **2010**, *4*, 380–386.

(20) Geng, X. M.; Niu, L.; Xing, Z. Y.; Song, R. S.; Liu, G. T.; Sun, M. T.; Cheng, G. S.; Zhou, H. J.; Liu, Z. H.; Zhang, Z. J.; Sun, L. F.; Xu, H. X.; Lu, L.; Liu, L. W. *Adv. Mater.* **2010**, *22*, 638–642.

(21) (a) Yang, H. F.; Shan, C. S.; Li, F. H.; Zhang, Q. X.; Han, D. X.; Niu, L. *J. Mater. Chem.* **2009**, *19*, 8856–8860. (b) Wang, H. L.; Hao, Q. L.; Yang, X. J.; Lu, L. D.; Wang, X. *ACS Appl. Mater. Interfaces* **2010**, *2*, 821–828.

(22) (a) Loh, K. P.; Bao, Q. L.; Ang, P. K.; Yang, J. X. *J. Mater. Chem.* **2010**, *20*, 2277–2289. (b) Wang, H. L.; Robinson, J. T.; Diankov, G.; Dai, H. J. *J. Am. Chem. Soc.* **2010**, *132*, 3270–3271.

(23) (a) Karyakin, A. A.; Karyakina, E. E.; Gorton, L. *Anal. Chem.* **2000**, *72*, 1720–1723. (b) Wang, G.; Zhou, J. H.; Li, J. H. *Biosens. Bioelectron.* **2007**, *22*, 2921–2925.

(24) Lukachova, L. V.; Kotel'nikova, E. A.; D'Ottavi, D.; Shkerin, E. A.; Karyakina, E. E.; Moscone, D.; Palleschi, G.; Curulli, A. *Bioelectrochemistry* **2002**, *55*, 145–148.

(25) (a) Kumar, S. S.; Joseph, J.; Phani, K. L. *Chem. Mater.* **2007**, *19*, 4722–4730. (b) Song, Y. Y.; Zhang, K.; Xia, X. H. *Appl. Phys. Lett.* **2006**, *88*, 53112–53113. (c) Uemura, T.; Kitagawa, S. *J. Am. Chem. Soc.* **2003**, *125*, 7814–7816. (d) Bai, J.; Qi, B.; Ndamanisha, J. C.; Guo, L. P. *Microporous Mesoporous Mater.* **2009**, *119*, 193–199. (e) Zou, Y. J.; Sun, L. X.; Xu, F. *Biosens. Bioelectron.* **2007**, *22*, 2669–2674.

(26) Zhang, D.; Zhang, K.; Yao, Y. L.; Xia, X. H.; Chen, H. Y. *Langmuir* **2004**, *20*, 7303–7307. Li, J.; Qiu, J. D.; Xu, J. J.; Chen, H. Y.; Xia, X. H. *Adv. Funct. Mater.* **2007**, *17*, 1574–1580.

(27) Li, Z. F.; Chen, J. H.; Li, W.; Chen, K.; Nie, L. H.; Yao, S. Z. *J. Electroanal. Chem.* **2007**, *603*, 59–66.

(28) Hummers, W. S.; Offeman, R. E. *J. Am. Chem. Soc.* **1958**, *80*, 1339–1339.

(29) Li, D.; Muller, M. B.; Gilje, S.; Kaner, R. B.; Wallace, G. G. *Nat. Nanotechnol.* **2008**, *3*, 101–105.

(30) Zhai, J. F.; Zhai, Y. M.; Wang, L.; Dong, S. J. *Inorg. Chem.* **2008**, *47*, 7071–7073.

(31) Cao, A. N.; Liu, Z.; Chu, S. S.; Wu, M. H.; Ye, Z. M.; Cai, Z. W.; Chang, Y. L.; Wang, S. F.; Gong, Q. H.; Liu, Y. F. *Adv. Mater.* **2009**, *22*, 103–106.

(32) Wu, X. L.; Cao, M. H.; Hu, C. W.; He, X. Y. *Cryst. Growth Des.* **2006**, *6*, 26–28.

(33) Cong, H. P.; He, J. J.; Lu, Y.; Yu, S. H. *Small* **2010**, *6*, 169–173.

(34) Uemura, T.; Ohba, M.; Kitagawa, S. *Inorg. Chem.* **2004**, *43*, 7339–7345.

(35) Yatsimirskii, K. B.; Nemoshkalenko, V. V.; Nazarenko, Y. P.; Aleshin, V. G.; Zhilinskaya, V. V.; Tomashevsky, N. A. *J. Electron Spectrosc. Relat. Phenom.* **1977**, *10*, 239–245.

(36) Li, F. H.; Song, J. F.; Yang, H. F.; Gan, S. Y.; Zhang, Q. X.; Han, D. X.; Ivaska, A.; Niu, L. *Nanotechnology* **2009**, *24*, 1765–1770.

(37) Han, S. F.; Chen, Y. M.; Pang, R.; Wan, P. Y. *Ind. Eng. Chem. Res.* **2007**, *46*, 68476851.

(38) McAllister, M. J.; Li, J. L.; Adamson, D. H.; Schniepp, H. C.; Abdala, A. A.; Liu, J.; Herrera-Alonso, M.; Milius, D. L.; Car, R.; Prud'homme, R. K.; Aksay, I. A. *Chem. Mater.* **2007**, *19*, 4396–4404.

(39) Agnihotry, S. A.; Singh, P.; Joshi, A. G.; Singh, D. P.; Sood, K. N.; Shivaprasad, S. M. *Electrochim. Acta* **2006**, *51*, 4291–4301.

(40) Yang, H. F.; Li, F. H.; Shan, C. S.; Han, D. X.; Zhang, Q. X.; Niu, L.; Ivaska, A. *J. Mater. Chem.* **2009**, *19*, 4632–4638.

(41) Park, S.; An, J.; Jung, I.; Piner, R. D.; An, S. J.; Li, X.; Velamakanni, A.; Ruoff, R. S. *Nano Lett.* **2009**, *9*, 1593–1597.

(42) Stankovich, S.; Dikin, D. A.; Piner, R. D.; Kohlhaas, K. A.; Kleinhammes, A.; Jia, Y.; Wu, Y.; Nguyen, S. T.; Ruoff, R. S. *Carbon* **2007**, *45*, 1558–1565.

(43) (a) Zhang, J. L.; Yang, H. J.; Shen, G. X.; Cheng, P.; Zhang, J. Y.; Guo, S. W. *Chem. Commun.* **2010**, *46*, 1112–1114. (b) Pham, V. H.; Cuong, T. V.; Nguyen-Phan, T. D.; Pham, H. D.; Kim, E. J.; Hur, S. H.; Shin, E. W.; Kim, S.; Chung, J. S. *Chem. Commun.* **2010**, *46*, 4375–4377.

(44) Nossol, E.; Zarbin, A. J. G. *Adv. Funct. Mater.* **2009**, *19*, 3980–3986.

(45) Das, A.; Pisana, S.; Chakraborty, B.; Piscanec, S.; Saha, S. K.; Waghmare, U. V.; Novoselov, K. S.; Krishnamurthy, H. R.; Geim, A. K.; Ferrari, A. C.; Sood, A. K. *Nat. Nanotechnol.* **2008**, *3*, 210–215.

(46) Chikae, M.; Idegami, K.; Kerman, K.; Nagatani, N.; Ishikawa, M.; Takamura, Y.; Tamiya, E. *Electrochem. Commun.* **2006**, *8*, 1375–1380.

(47) Du, D.; Wang, M. H.; Qin, Y. H.; Lin, Y. H. *J. Mater. Chem.* **2010**, *20*, 1532–1537.

(48) Li, M. Y.; Zhao, G. Q.; Yue, Z. L.; Huang, S. S. *Microchim Acta* **2009**, *167*, 167–172.

(49) Zhai, J. F.; Zhai, Y. M.; Wen, D.; Dong, S. J. *Electroanalysis* **2009**, *21*, 2207–2212.

AM100372M